

1 **Carbon isotope ratios of coccolith-associated polysaccharides of *Emiliana huxleyi* as**
2 **a function of growth rate and CO₂ concentration**

3

4 Elise B. Wilkes^{a*}, Renee B.Y. Lee^{b,c}, Harry L. O. McClelland^{b,d}, Rosalind E. M.
5 Rickaby^b, and Ann Pearson^a

6 ^aDepartment of Earth and Planetary Sciences, Harvard University, Cambridge, MA, USA

7 ^bDepartment of Earth Sciences, University of Oxford, Oxford, UK.

8 ^cSchool of Biological Sciences, University of Reading, Reading, UK

9 ^dDepartment of Earth and Planetary Sciences, Washington University in St. Louis, MO,
10 USA

11 *elisewilkes@fas.harvard.edu

12

13 **Abstract**

14 The calcite plates, or coccoliths, of haptophyte algae including *Emiliana huxleyi* are
15 formed in intracellular vesicles in association with water-soluble acidic polysaccharides.

16 These coccolith-associated polysaccharides (CAPs) are involved in regulating coccolith
17 formation and have been recovered from sediment samples dating back to ~180 Ma.

18 Paired measurements of the carbon isotopic compositions of CAPs and coccolith calcite
19 have been proposed as a novel paleo-*p*CO₂ barometer, but additional proxy validation and

20 development are still required. Here we present culture results quantifying carbon
21 isotopic offsets between CAPs and other cellular components: bulk organic biomass,

22 alkenones, and calcite. *E. huxleyi* was grown in nitrate-limited chemostat experiments at
23 growth rates (μ) of 0.20-0.62 d⁻¹ and carbon dioxide concentrations of 10.7-17.6 μ mol

kg⁻¹. We find that CAPs are isotopically enriched by 4.5 to 10.1‰ relative to bulk organic carbon, exhibiting smaller isotopic offsets at faster growth rates and lower CO₂ concentrations. This variability suggests that CAPs record a complementary signature of past growth conditions with different sensitivity than alkenones or coccolith calcite. By measuring the isotopic compositions of all three molecules and minerals of self-consistent origin, the ratio $\mu/[\text{CO}_{2(\text{aq})}]$ may be reconstructed with fewer assumptions than current approaches.

Keywords: polysaccharide, coccolith, alkenone, isotope fractionation, chemostat, climate proxy, *E. huxleyi*, paleobarometry

1. Introduction

Emiliana huxleyi is a cosmopolitan, bloom-forming marine algal species that uses dissolved inorganic carbon (DIC) for calcification and photosynthesis (Westbroek, 1993). It is the dominant coccolithophore in modern oceans, capable of producing calcifying plates (“coccoliths”) that interlock around the cell (De Vargas et al., 2007, Henriksen and Stipp, 2009). The stable carbon and oxygen isotopic compositions of fossilized coccoliths have been used to reconstruct paleoclimatic and evolutionary events (Stoll, 2005, Rickaby et al., 2007, Hermoso et al., 2009, Bolton and Stoll, 2013). *E. huxleyi* also synthesizes long-chain unsaturated ketones called alkenones that are preserved in the geologic record and used as paleotemperature and paleobarometry ($p\text{CO}_2$) proxies (e.g., Volkman et al., 1980, Marchal et al., 2002, Pagani et al., 2005, Zhang et al., 2013, Brassell, 2014). Although *E. huxleyi* only became dominant in the fossil record around 70 ka, alkenones first appear in Cretaceous sediments, and fossil

47 coccoliths have been dated to the Late Triassic (Thierstein et al., 1977, Farrimond et al.,
48 1986, Bown et al., 1987).

49 Coccolith precipitation occurs intracellularly in vesicles that maintain a controlled
50 chemical composition (Henriksen and Stipp, 2009). Coccolithogenesis begins with the
51 formation of precursor organic templates that provide a framework of binding sites for
52 crystal nucleation and growth (Young et al., 2003). The calcite crystals grow to form
53 complex units, with mineral expression regulated by acidic polysaccharides (Marsh,
54 2002). Completed coccoliths and coccolith-associated polysaccharides (CAPs) trapped
55 within ultimately are expelled to the outside of the cell. *E. huxleyi* contains one type of
56 CAP, consisting of a polymeric mannose backbone with sidechains of galacturonic acid
57 and ester-bound sulfate groups (De Jong et al., 1976, Fichtinger-Schepman et al., 1981,
58 Kok et al., 1986). Another coccolithophore species, *Pleurochrysis carterae*, contains
59 three types of CAPs, with both galacturonic and glucuronic moieties (Marsh et al., 1994,
60 Marsh et al., 2003). CAPs interact with the carbonate chemistry of the coccolith vesicle
61 through the carboxyl groups of the uronic acid residues, which can shed protons to
62 preferentially bind calcium cations (Borman et al., 1982).

63 CAPs are increasingly being used to study the interplay between the ambient
64 environment and the carbonate chemistry of intracellular carbon pools (Henriksen and
65 Stipp, 2009, Lee et al., 2016, Rickaby et al., 2016). Lee et al. (2016) extracted intact
66 CAPs from both modern cultures and fossil coccoliths dating back to ~180 Ma. The
67 uronic acid contents of these extracts correlated with the predicted internal saturation
68 state of the coccolith vesicle in modern cultures and approximately tracked Phanerozoic
69 $p\text{CO}_2$ reconstructions obtained from other paleo-proxies (Lee et al., 2016).

The stable carbon isotopic composition of CAPs ($\delta^{13}\text{C}_{\text{CAP}}$) may provide further complementary information. $\delta^{13}\text{C}_{\text{CAP}}$ values, measured in conjunction with coccolith calcite $\delta^{13}\text{C}$ values, have been proposed as a novel paleobarometer for ancient $p\text{CO}_2$ (Hermoso, 2014, McClelland et al., 2017). Such application assumes that $\delta^{13}\text{C}_{\text{CAP}}$ values predictably track $\delta^{13}\text{C}_{\text{biomass}}$ values and can be used to calculate the isotope fractionation accompanying photosynthesis (ϵ_{P} values; Freeman and Hayes, 1992). Preliminary work shows that $\delta^{13}\text{C}_{\text{CAP}}$ values are measurable (R.B.Y. Lee, unpublished, McClelland et al., 2015), but no paired measurements of $\delta^{13}\text{C}_{\text{CAP}}$ values and bulk organic carbon have been reported. In this study we measure the $\delta^{13}\text{C}$ values of CAPs, bulk cellular organic carbon, calcite, and alkenones of *E. huxleyi* grown in nitrate-limited chemostat cultures. Results are analyzed as a function of growth rate and CO_2 availability, with all other culture conditions held constant.

2. Materials and methods

2.1 Chemostat culture methods

A coccolith-bearing strain of *E. huxleyi* (CCMP3266) was grown in a nitrate-limited chemostat at a constant temperature of 18°C. Experimental conditions were selected to mimic the cultures of Bidigare et al. (1997) and employed the chemostat system described in Wilkes et al. (2017). Cool-white fluorescent light was supplied continuously with a saturating photon flux density of $\sim 150 \mu\text{mol photons m}^{-2} \text{ s}^{-1}$ (400-700 nm radiation). The vessel was stirred at 50 rpm. The growth medium consisted of 0.2 μm -filtered and autoclaved Gulf of Maine natural seawater enriched with metals and vitamins according to L1 medium (Guillard and Hargraves, 1993). Initial nitrate and

phosphate concentrations were adjusted to approximately 100 μM and 36 μM , respectively. Four different growth rates (μ ; 0.20-0.62 d^{-1} ; Table 1) were achieved by adjusting the dilution rate.

Cell densities were monitored daily by OD_{600} and by cell counts using a hemocytometer counting chamber and a light microscope. Residual nitrate and phosphate concentrations were determined spectrophotometrically on 0.22 μm -filtered and refrigerated samples using the resorcinol (Zhang and Fischer, 2006) and mixed molybdate (Strickland and Parsons, 1968) methods, respectively. Daily sample removal never exceeded 4% of the culture volume to minimize perturbations to steady-state conditions.

2.2. Carbonate system chemistry

Four CO_2 concentrations from 10.7-17.6 $\mu\text{mol kg}^{-1}$ (Table 1) were maintained by bubbling with mixtures of tank CO_2 ($\delta^{13}\text{C}_{\text{CO}_2} = -38.58 \pm 0.03\text{‰}$) and 4:1 $\text{N}_2:\text{O}_2$. pH was monitored continuously using an in-process pH probe (EasyFerm Plus, Hamilton). Total dissolved inorganic carbon (DIC) and alkalinity samples were taken daily during the steady-state phase of each experiment (final 3-6 days). Samples for DIC were collected without headspace, poisoned with 0.2 w/w % sodium azide, and stored in darkness at 4°C. DIC was converted to CO_2 by acidification with H_3PO_4 , purified on a vacuum line, and quantified manometrically. Total alkalinity was determined by Gran titration with 0.01 N HCl solution prepared in a 0.7 M NaCl background (Gran, 1952, Dickson et al., 2007), using certified reference materials supplied by A.G. Dickson (Scripps Institution of Oceanography) to monitor precision. The carbonate system was calculated from DIC,

pH, phosphate, temperature, and salinity using CO2SYS (Lewis and Wallace, 1998, van Heuven et al., 2011, Table S1) and the dissociation constants of Mehrbach et al. (1973), as refitted by Dickson and Millero (1987), and Dickson (1990). The combined uncertainties in calculated inorganic carbon speciation were estimated numerically following Bevington and Robinson (2003).

2.3. Isotopic Analysis

Cells were pelleted by centrifugation and stored at -80°C. Values of $\delta^{13}\text{C}_{\text{biomass}}$ were measured on thawed, acidified (1N HCl) and dried (60°C) samples using an elemental analyzer interfaced to a continuous flow isotope ratio mass spectrometer (EA-IRMS; UC Davis Stable Isotope Facility). Alkenone $\delta^{13}\text{C}$ values were measured from total lipid extracts (Bligh and Dyer, 1959) using gas chromatography-isotope ratio mass spectrometry (GC-IRMS: Thermo Scientific Delta V Advantage interfaced to a Trace GC Ultra via a GC Isolink). Alkenones were separated on a 60-m DB1-MS capillary column using the following oven ramp program: ramp from 65-110°C at 40°C min⁻¹ and hold 2 minutes, ramp to 270°C at 40°C min⁻¹, ramp to 320°C at 2°C min⁻¹ and hold 36 minutes. Values of $\delta^{13}\text{C}$ were measured and averaged for C_{37:3} and C_{37:2} alkenones (peak sizes, 0.5V-5V, m/z 44) using *n*-C32, *n*-C38, and *n*-C41 alkane external standards.

CAPs were isolated from freeze-dried biomass pellets according to the protocol described in Lee et al. (2016). Briefly, cells were cleaned with 1% v/v Triton X-100, 4.5% v/v NaOCl in 0.05 M NaHCO₃. The coccoliths were centrifuged through a gradient of Ludox TM-50 colloidal silica (Sigma-Aldrich) layered with 20% w/v sucrose. After

additional rinses with NH_4HCO_3 , the pellet was decalcified with 0.5 M EDTA (pH 8.0, 12 h) and sonicated. Insoluble residues were removed by centrifugation and the supernatant was diafiltered with an Amicon Ultra-4 centrifugal filter unit (Millipore). The CAP was isolated by anion exchange liquid chromatography using a HiTrap DEAE FF (GE Healthcare). CAP $\delta^{13}\text{C}$ values were analyzed by spooling wire micro-combustion isotope ratio mass spectrometry (SWiM-IRMS, Harvard University) using a pectin standard; full process blanks were assessed using both MilliQ water and the pectin standard.

$\delta^{13}\text{C}$ values of DIC were measured at Woods Hole Oceanographic Institution on CO_2 gas samples collected in Pyrex tubes following purification and DIC quantification on a vacuum line. Carbon isotope compositions of coccolith calcite were measured using a Thermo Delta V Advantage isotope ratio mass spectrometer fitted to a Kiel IV carbonate device (University of Oxford). All measured isotope values are reported on the international V-PDB scale. Carbon isotope fractionations between different cellular constituents are reported as simple linear differences ($\Delta\delta_{(A-B)} = \delta^{13}\text{C}_A - \delta^{13}\text{C}_B$) and as epsilon values (following Freeman and Hayes, 1992, Zeebe and Wolf-Gladrow, 2001):

$$\epsilon_{(A-B)} = (\delta^{13}\text{C}_A - \delta^{13}\text{C}_B) / (1 + \delta^{13}\text{C}_B / 10^3).$$

3. Results

3.1. Chemostat Cultures

Each experiment reached steady state for all measured variables 7-12 days after setting the initial conditions (dilution rate and CO_2 combination). Measurements over the subsequent 3-6 days were treated as replicates and averaged. Final cell densities were

approximately 3×10^6 cells ml^{-1} across experiments (Table S2), as expected based on the low half-saturation constant for nitrate ($K_M = 0.35 \mu\text{M}$, Perrin et al. 2016) relative to the initial concentration in the growth medium ($100 \mu\text{M}$). Routine monitoring of residual nitrate concentrations indicated at least a 25-fold reduction from the concentration in the feed media, yielding residual molar N:P ratios of less than 0.2 in all experiments (Table S2). Dissolved CO_2 concentrations (Table 1) were within the ranges of both the modern ocean ($\sim 8\text{-}30 \mu\text{mol kg}^{-1}$) and prior chemostat culture investigations of *E. huxleyi* ($9.6\text{-}274.1 \mu\text{mol kg}^{-1}$; Bidigare et al., 1997, Popp et al., 1998a,b). Growth rates (μ , Table 1) were between 16 and 51% of the maximum growth rates achieved in nutrient-replete batch cultures ($\mu_{\text{max}} = 1.22 \text{ d}^{-1}$, Hermoso et al., 2016a).

3.2. Carbon isotopic compositions of cellular constituents and DIC

Coccolith calcite was the most ^{13}C -enriched cellular component, with $\delta^{13}\text{C}$ values ranging from -15.4 to -8.3‰ (Table 1). CAPs were the most enriched organic component (-39.5 to -38.2‰), followed by bulk biomass (-48.2 to -39.5‰) and alkenones (-51.5 to -42.4‰) (Table 1). The strongly negative absolute values of $\delta^{13}\text{C}$ in all carbon pools reflect the influence of the tank CO_2 ($-38.58 \pm 0.03\text{‰}$) used to adjust the seawater carbonate chemistry.

$\delta^{13}\text{C}_{\text{DIC}}$ values were measured for five consecutive sampling days at steady state during Experiment #1, with a mean value of $\delta^{13}\text{C}_{\text{DIC}} = -18.3 \pm 0.2\text{‰}$. The isotopic composition of the dissolved CO_2 (-27.8‰) was calculated from $\delta^{13}\text{C}_{\text{DIC}}$ and carbonate speciation (Zeebe and Wolf-Gladrow, 2001), using the fractionation factors of Mook et al. (1974) and Zhang et al. (1995). Unfortunately, due to a technical malfunction, $\delta^{13}\text{C}_{\text{DIC}}$

measurements are unavailable for the remaining three experiments. However, the measurements from Experiment #1 confirm that the fractionations expressed between DIC, biomass, and coccolith calcite are consistent with literature ranges. Photosynthetic carbon isotope fractionation (ϵ_p) was $21.4 \pm 1.5\text{‰}$, calculated relative to CO_2 as the inorganic carbon source, or 31.4‰ calculated relative to total DIC. This result agrees with Bidigare et al. (1997; Fig. S1a), and falls within theoretical bounds established for eukaryotic phytoplankton (Goericke et al., 1994, Popp et al., 1998a; Wilkes et al., 2017). Interestingly, coccolith calcite is enriched by 2.9‰ relative to DIC in Experiment #1 (and 1.9‰ relative to thermodynamic predictions for inorganically-precipitated calcite, Romanek et al., 1992). This nearly 3‰ enrichment is at the upper end of the range reported from prior batch cultures of *E. huxleyi* ($\Delta\delta^{13}\text{C}_{\text{calcite-DIC}} = -4.2$ to 3‰ ; Rost et al., 2002, Ziveri et al., 2003, Hermoso et al., 2016b, Katz et al., 2017, McClelland et al., 2017), likely reflecting differences in nutrient conditions and carbonate system manipulation between studies.

3.3. Isotopic sensitivities to changing growth rate and $[\text{CO}_{2(\text{aq})}]$

The $\delta^{13}\text{C}$ values of bulk cellular biomass, calcite, and alkenones are influenced by the ratio $\mu/[\text{CO}_{2(\text{aq})}]$ (Bidigare et al., 1997, Popp et al., 1998a,b, Riebesell et al., 2000, Tchernov et al., 2014, Hermoso et al., 2016b). These three cellular components, as well as CAPs, display strong linear relationships with respect to $\mu/[\text{CO}_{2(\text{aq})}]$ in this study ($r^2 > 0.90$, $p < 0.05$, Fig. 1a; Fig. S1b). The $\delta^{13}\text{C}$ values for each cellular pool grow increasingly ^{13}C -enriched with increasing $\mu/[\text{CO}_{2(\text{aq})}]$, although not all pools have the same slope (Fig. 1a). $\delta^{13}\text{C}_{\text{biomass}}$ and $\delta^{13}\text{C}_{\text{alkenone}}$ values display the greatest sensitivity to

208 $\mu/[CO_{2(aq)}]$, with nearly identical slopes of 190 and 202 kg d $\mu mol^{-1} \text{‰}^{-1}$, respectively.
 209 $\delta^{13}C_{calcite}$ values display slightly less sensitivity with a slope of 157. $\delta^{13}C_{CAP}$ values
 210 respond least sensitively to $\mu/[CO_{2(aq)}]$, with a slope of 75 kg d $\mu mol^{-1} \text{‰}^{-1}$. When the
 211 $\delta^{13}C$ values of alkenones and CAPs are compared to the bulk phases (calcite and
 212 biomass) the slopes of the cross-plots are approximately 1 and 0.5, respectively (Fig.
 213 1b,c).

214 The differences in isotopic sensitivities to $\mu/[CO_{2(aq)}]$ are apparent by examining
 215 $\Delta\delta$ values, the isotopic differences between any two cellular carbon pools (Fig. 2).
 216 $\Delta\delta^{13}C_{calcite-CAP}$ and $\Delta\delta^{13}C_{CAP-biomass}$ values both display robust linear relationships: with
 217 increasing $\mu/[CO_{2(aq)}]$, $\Delta\delta^{13}C_{calcite-CAP}$ values increase from 22.7 to 26.7‰ (Fig. 2a) while
 218 $\Delta\delta^{13}C_{CAP-biomass}$ values decrease from 10.1 to 4.5‰ (Fig. 2b). These opposing trends are
 219 also evident in Figure 1: $\delta^{13}C_{CAP}$ values approach $\delta^{13}C_{biomass}$ values and diverge from
 220 $\delta^{13}C_{calcite}$ values in the limit of faster growth or lower $[CO_{2(aq)}]$.

221 Consistent with prior work, $\Delta\delta^{13}C_{biomass-alkenone}$ values are constant within error
 222 across all four experiments, with a mean value of $3.5 \pm 0.5\text{‰}$ (Table 2), and display no
 223 significant linear dependence on $\mu/[CO_{2(aq)}]$ ($r^2 = 0.20$, $p > 0.05$, Fig. 2c). Prior *E. huxleyi*
 224 chemostat cultures under analogous conditions ($\mu = 0.2\text{-}0.6 \text{ d}^{-1}$, 18°C, nitrate-limited)
 225 similarly exhibited $\Delta\delta^{13}C_{biomass-alkenone}$ values (3.5-5.2‰) with no clear dependence on
 226 growth rate (Popp et al., 1998b). $\Delta\delta^{13}C_{calcite-biomass}$ values also do not display a statistically
 227 significant response to $\mu/[CO_{2(aq)}]$ ($p > 0.05$, Fig. 2d; mean $32.3 \pm 0.7\text{‰}$). By analogy,
 228 therefore, the difference $\Delta\delta^{13}C_{calcite-alkenone}$ would also be statistically constant over the
 229 range of the experiments; and collectively, the $\Delta\delta$ values indicate that biomass, alkenone,

and calcite $\delta^{13}\text{C}$ values all effectively respond equally to $\mu/[\text{CO}_{2(\text{aq})}]$ (Fig. 1, 2). Only $\delta^{13}\text{C}_{\text{CAP}}$ values have a different $\mu/[\text{CO}_{2(\text{aq})}]$ sensitivity.

Maximum isotopic offsets between substrates and carbon pools occur in the limit of infinite $[\text{CO}_{2(\text{aq})}]$ or zero growth (Goericke et al., 1994, Laws et al., 1995). For example, ε_{P} values ($\approx \Delta\delta^{13}\text{C}_{\text{CO}_2\text{-biomass}}$) have an expected intercept of approximately 25‰, inferred from prior chemostat cultures of eukaryotic algae including *E. huxleyi* (Popp et al., 1998a). This value has been interpreted as the maximum fractionation accompanying enzymatic carbon fixation (ε_{f}). Although we were unable to measure $\delta^{13}\text{C}_{\text{DIC}}$ values for three of our experiments and thus cannot directly solve the $\varepsilon_{\text{P}} = \varepsilon_{\text{f}} - \mu/[\text{CO}_{2(\text{aq})}]$ equation in this study, the analogous intercept values for other carbon pools may provide insight into the inherent isotope effects of the governing reactions. $\Delta\delta^{13}\text{C}_{\text{calcite-CAP}}$ approaches an intercept of approximately 22‰, $\Delta\delta^{13}\text{C}_{\text{CAP-biomass}}$ approaches 11‰, $\Delta\delta^{13}\text{C}_{\text{biomass-alkenone}}$ approaches 4‰, and $\Delta\delta^{13}\text{C}_{\text{calcite-biomass}}$ approaches 33‰.

4. Discussion

4.1. Intracellular carbon isotope patterns – bulk classes

The isotopic ordering among compound classes matches general expectations for photoautotrophs. Organic carbon is ^{13}C -depleted relative to inorganic carbon (DIC and coccolith calcite) in our samples due to kinetic discrimination against $^{13}\text{CO}_2$ during photosynthesis (e.g., Goericke et al., 1994). Within the organic carbon pools, typical intracellular isotopic ordering also prevails: carbohydrates are more enriched in ^{13}C than total cellular biomass, while lipids are ^{13}C -depleted (Wong et al., 1975, Sakata et al., 1997, Hayes, 2001). This consistent isotopic pattern ($\delta^{13}\text{C}_{\text{CAP}} > \delta^{13}\text{C}_{\text{biomass}} > \delta^{13}\text{C}_{\text{alkenone}}$)

can be explained by a biosynthetic reaction network in which simple carbohydrates, used to synthesize CAPs, are the first compounds generated, while downstream kinetic processes discriminate against ^{13}C and produce relatively ^{13}C -depleted products including alkenones (Hayes, 2001).

All $\Delta\delta$ values (Fig. 2) are also consistent with expectations. Our mean $\Delta\delta^{13}\text{C}_{\text{biomass-alkenones}}$ value of $3.5 \pm 0.5\text{‰}$ (equivalent to $\epsilon_{\text{biomass-alkenones}} = 3.7\text{‰}$; Table S3) is within error, although on the lower end, of the 3.8-4.2‰ corrections that have been implemented in paleobarometry studies (Jasper and Hayes, 1990, Jasper, 1994, Pagani, 2005, Bijl et al., 2010, Seki et al., 2010) and is typical of the expressed fractionation for acetogenic lipids relative to total biomass (*e.g.*, Hayes, 2001).

Paired measurements of calcite and biomass $\delta^{13}\text{C}$ values from the same study are rare. Our mean $\Delta\delta^{13}\text{C}_{\text{calcite-biomass}}$ value of $32.3 \pm 0.7\text{‰}$ (equivalent to $\epsilon_{\text{calcite-biomass}} = 33.8 \pm 0.9\text{‰}$; Table S3) exceeds the values measured in two nutrient-replete batch culture studies of *E. huxleyi* ($\Delta\delta^{13}\text{C}_{\text{calcite-biomass}} = 15.3\text{--}28.8\text{‰}$, Rost et al., 2002, McClelland et al., 2017), but the difference must partially reflect the larger ϵ_{P} values obtained in nitrate-limited chemostats ($\epsilon_{\text{P}} = 21.4\text{‰}$, Experiment #1; 17.2-24.9‰ Bidigare et al., 1997, Fig. S1a) relative to those from the batch cultures ($\epsilon_{\text{P}} = 6.7\text{--}17.1\text{‰}$, Rost et al., 2002, McClelland et al., 2017). The larger fractionations in our study may also result from the continuous, relatively high light conditions employed (associated with larger ϵ_{P} values; Rost et al., 2002, Holtz et al., 2017) and differences in carbonate system manipulation between studies (McClelland et al., 2017).

No prior investigations have characterized the carbon isotope fractionation between CAPs and other cellular pools; and interestingly, the $\Delta\delta$ values we observe for

CAPs appear to be different from expectations for bulk carbohydrates. Bulk carbohydrates can be up to 3-4‰ enriched relative to total biomass for photoautotrophs, but more commonly are thought to be on average 1-2‰ enriched (Abelson and Hoering, 1961, Coffin et al., 1990, Macko et al., 1990, Hayes, 2001). However, analyses of individual monosaccharides indicate substantial isotopic heterogeneity within the bulk carbohydrate pool, with some being significantly enriched in ^{13}C (van Dongen et al., 2002, Teece and Fogel, 2007). Our $\Delta\delta^{13}\text{C}_{\text{CAP-biomass}}$ values (4.5 to 10.1‰, Table 2) fall within ranges observed for individual monosaccharides in marine and freshwater algae (0-9‰ for unicellular algae, and up to 13‰ for the macroalgal species *Ulva lactuca*; van Dongen et al., 2002, Teece and Fogel, 2007). Teece and Fogel (2007) measured $\delta^{13}\text{C}$ values for glucose and galactose from a batch culture of *E. huxleyi*, finding enrichments of 5 and 7‰ relative to biomass, respectively, and leading to predictions of $\Delta\delta^{13}\text{C}_{\text{CAP-biomass}}$ values ~6‰ (Benthien et al., 2007, Boller et al., 2011). Yet the most prevalent monomers within the CAP structure (mannose, galacturonic acid, and rhamnose; Fichtinger-Schepman, 1981) have not to date been isotopically characterized for this species. In a field specimen of *Ulva lactuca*, these monomers were ^{13}C -enriched relative to biomass by 10‰ (mannose), 13‰ (galactose), and 7‰ (rhamnose), respectively (Teece and Fogel, 2007). Because our $\Delta\delta^{13}\text{C}_{\text{CAP-biomass}}$ values of 4.5-10.1‰ are broadly consistent with these existing measurements, it is likely that $\delta^{13}\text{C}_{\text{CAP}}$ values are more ^{13}C -enriched than the mass-weighted average carbohydrate composition of the cells, perhaps to an even greater extent than predicted by Benthien et al. (2007) and Boller et al. (2011).

4.2. Linear isotopic responses to changing $\mu/[CO_{2(aq)}]$

The linear increase in $\delta^{13}C_{\text{biomass}}$ values with increasing $\mu/[CO_{2(aq)}]$ (Fig. 1) is consistent with predictions from simple algal models invoking primarily diffusive entry of CO_2 into the cell for photosynthetic fixation (*e.g.*, Freeman and Hayes, 1992, Laws et al., 1995). Bidigare et al. (1997) showed similar linear increases in $\delta^{13}C_{\text{biomass}}$ values under analogous chemostat growth conditions (Fig. S1b).

The parallel increase in $\delta^{13}C_{\text{calcite}}$ values with increasing $\mu/[CO_{2(aq)}]$ (Fig. 1) supports the hypothesis that a common physiological mechanism governs the isotopic signature of both calcite and biomass. Photosynthesis discriminates against ^{13}C in the chloroplast, producing depleted $\delta^{13}C_{\text{biomass}}$ values while simultaneously enriching ^{13}C in the remaining intracellular DIC pool. If this enriched DIC is also used for calcification, $\delta^{13}C_{\text{calcite}}$ and $\delta^{13}C_{\text{biomass}}$ values might both be expected to increase in response to increasing $\mu/[CO_{2(aq)}]$, consistent with our observed constant value for $\Delta\delta^{13}C_{\text{calcite-biomass}}$ ($32.3 \pm 0.7\text{‰}$; Table 2) and measurements of other lightly-calcifying coccolithophores (Hermoso et al., 2016b, McClelland et al., 2017). In species with higher ratios of particulate inorganic to organic carbon (high PIC:POC ratios), $\delta^{13}C_{\text{calcite}}$ values would instead be expected to decrease with increasing $\delta^{13}C_{\text{biomass}}$ values since the fractionation associated with calcite precipitation would obscure the chloroplast-derived fraction of the signal (Hermoso et al., 2016b, McClelland et al., 2017).

Similar reasoning also explains the linear responses of the organic compound classes (alkenones and CAPs) to $\mu/[CO_{2(aq)}]$, but it cannot explain why the slope of the $\delta^{13}C$ vs. $\mu/[CO_{2(aq)}]$ signature is not conserved in the CAPs (Fig. 1). Under high utilization of CO_2 (larger values for $\mu/[CO_{2(aq)}]$), $\delta^{13}C_{\text{CAP}}$ values appear to be approaching

$\delta^{13}\text{C}_{\text{biomass}}$ values, while at very low utilization, the value of $\Delta\delta^{13}\text{C}_{\text{CAP-biomass}}$ has a predicted maximum of 11‰ (y-axis intercept, Fig. 2b). This changing signature specifically indicates that $\delta^{13}\text{C}_{\text{CAP}}$ values are approximately half as sensitive as the other cellular components to the ratio $\mu/[\text{CO}_{2(\text{aq})}]$, and it points towards a more complex control on the isotopic composition of this polymer.

4.3. Physiological interpretation of $\delta^{13}\text{C}_{\text{CAP}}$ patterns

The fractionation between CAPs and biomass ($\Delta\delta^{13}\text{C}_{\text{CAP-biomass}}$) spans a 5.6‰ range without any compensatory change in $\Delta\delta^{13}\text{C}_{\text{alkenone-biomass}}$ values. This could occur if isotopically-distinct carbohydrate pools exist within *E. huxleyi* and the relative amount of carbon flowing to these pools varies systematically with growth conditions. Simple assumptions about cellular composition are used to illustrate this hypothesis, following Hayes (2001).

$\delta^{13}\text{C}_{\text{biomass}}$ values reflect the fractional allocation of cellular carbon to the major organic compound classes, as well as the mass-weighted average isotopic composition of each class (Eqn. 1). The subscripts in Equation 1 correspond to proteins, carbohydrates, and lipids, respectively; f is the fractional flux of fixed carbon flowing to each compound class at steady-state. We also assume that the bulk carbohydrate pool, denoted δ_{carb} , results from the balance of two distinct carbohydrate fractions: acidic polysaccharides (f_{CAP}) and other saccharides (f_{sacc}) (Eqn. 2).

$$\delta_{\text{biomass}} = f_{\text{prot}}\delta_{\text{prot}} + f_{\text{carb}}\delta_{\text{carb}} + f_{\text{lip}}\delta_{\text{lip}} \quad (1)$$

$$\delta_{\text{carb}} = f_{\text{CAP}}\delta_{\text{CAP}} + f_{\text{sacc}}\delta_{\text{sacc}} \quad (2)$$

344 Values of δ_{biomass} and δ_{CAP} correspond to the values listed in Table 1, and δ_{lip}
 345 values are estimated to be 4‰ ^{13}C -depleted relative to biomass ($\delta_{\text{lip}} = \delta_{\text{biomass}} - 4\text{‰}$, Eqn.
 346 3, Table 3) by analogy with our $\delta^{13}\text{C}_{\text{alkenones}}$ measurements and other consensus
 347 observations (*e.g.*, Schouten et al., 1998, Laws et al., 2001). Alkenones and total lipids
 348 are assumed to be isotopically equivalent because alkenones represent a significant
 349 fraction of the lipids synthesized in *E. huxleyi*. Quantitative analyses of carbon fluxes
 350 show that up to 18% of photosynthetic carbon is dedicated to alkenones in cells harvested
 351 from batch cultures (Tsuji et al., 2015). We further assume that proteins and biomass
 352 would be isotopically equal ($\delta_{\text{prot}} = \delta_{\text{biomass}}$), since proteins are expected to represent the
 353 majority of total cell carbon (*e.g.*, Hayes, 2001, Tang et al., 2017). Finally, δ_{carb} ,
 354 representing the total combined carbohydrate fraction in the cell, is assumed to be
 355 enriched by 4‰ relative to biomass ($\delta_{\text{carb}} = \delta_{\text{biomass}} + 4\text{‰}$, Eqn. 3, Table 3). This
 356 assumption is at the upper end of the range reported for bulk carbohydrates in other
 357 autotrophs (Wong et al., 1975, van der Meer et al., 2001, van Dongen et al., 2002).

$$\delta_{\text{biomass}} = f_{\text{prot}}(\delta_{\text{biomass}}) + f_{\text{carb}}(\delta_{\text{biomass}} + 4\text{‰}) + f_{\text{lip}}(\delta_{\text{biomass}} - 4\text{‰}) \quad (3)$$

359 Solving Eqn 3 requires an estimate of one fractional flux, so we estimate $f_{\text{lip}} =$
 360 0.25 by considering how biosynthesis affects the carbon isotopic composition of *n*-alkyl
 361 lipids. Acetyl-coenzyme A (CoA) is produced from the decarboxylation of pyruvate by
 362 the enzyme pyruvate dehydrogenase. This step is accompanied by an isotope effect of
 363 $\sim 23\text{‰}$, generating a ^{13}C -depleted carboxyl group relative to the methyl group in
 364 acetyl-CoA (Monson and Hayes, 1982, Hayes, 2001). This translates to a $\sim 12\text{‰}$
 365 depletion for the overall acetyl-CoA molecule relative to pyruvate. However, the net
 366 isotopic composition of the resulting acetogenic lipids relative to biomass is controlled by

the branching ratio of pyruvate destined for lipid synthesis vs. that used directly, either for cellular biosynthesis or for carboxylation to oxaloacetate by anaplerotic reactions. In the absence of anaplerotic reactions, an expressed 4‰ depletion in lipids relative to biomass would indicate allocation of ~33% of pyruvate to lipid synthesis, but accounting for additional anaplerotic fluxes (*e.g.*, Tang et al., 2017) decreases this estimate to ~25%.

Proteins and carbohydrates must together constitute the remaining biomass (75%) in Eqn. 3, allowing us to solve for the remaining unknowns. We find that bulk cellular carbon allocation remains invariant across our experiments: $f_{lip} = 0.25$, $f_{prot} = 0.5$, $f_{carb} = 0.25$ (Table 3, Fig. 3a,b). The fractional allocation to CAPs (f_{CAP}) versus other saccharides (f_{sacc}) is calculated by assuming a net fractionation factor between the two pools ($\Delta\delta_{CAP-sacc}$) of 7‰ (Eqn. 4, Table 3). This value corresponds to the maximum $\Delta\delta^{13}C_{CAP-biomass}$ value of 11‰ inferred from the y-intercept of Fig. 2b, corrected by 4‰ to account for our assumption that δ_{carb} is 4‰ enriched relative to $\delta_{biomass}$ (Eqn. 3).

$$\delta_{carb} = \delta_{biomass} + 4‰ = f_{CAP}\delta_{CAP} + (1-f_{CAP})(\delta_{CAP}-7‰) \quad (4)$$

The f_{CAP} results (Table 3) indicate that the total cellular carbon allocation to CAPs increases from 3.5 to 22.8% from Experiment #1 to #4, in agreement with ^{14}C -labeling experiments showing that ~15-20% of fixed carbon is used for the synthesis of acidic polysaccharides in *E. huxleyi* (Kayano and Shiraiwa 2009, Tsuji et al., 2015, Taylor et al., 2017).

To test the sensitivity of our model results, other plausible choices of δ_{prot} and δ_{carb} inputs are evaluated in Table 3, Fig. 3b, and Fig. S2; all cases suggest that *E. huxleyi* produces more CAPs relative to other carbohydrates as $\mu/[CO_{2(aq)}]$ increases (Table 3, Fig. 3a,b). It remains unknown whether this response in our cultures is a consequence of

the faster growth rate or the relatively lower CO₂ concentrations under these conditions. Several studies imply that *E. huxleyi* regulates carbon flow among CAPs, neutral polysaccharides, and low molecular weight (LMW) metabolites in response to changing growth conditions (Kayano and Shiraiwa, 2009, Borchard and Engel, 2012, Chow et al., 2015). Most of these studies have been conducted with batch cultures or phosphorous-limited chemostat cultures, so as yet no corroborating evidence for nitrate-limited conditions exists. However, our estimates are consistent with ¹⁴C-labeling experiments with the green alga *Dunaliella tertiolecta* in nitrate-limited chemostat cultures (Halsey et al., 2011), which showed that at faster growth rates, proportionally more ¹⁴C is allocated to polysaccharides, and at slower growth rates, more ¹⁴C is allocated to LMW metabolites. For *E. huxleyi*, this may reflect a strategy by the cell to support calcification when the intracellular carbon pool is relatively depleted. Alternatively, our data might imply that CAPs are synthesized from proportionally more recycled cellular carbon with increasing growth rates. If proteins are recycled for the synthesis of CAPs, and $\delta_{\text{prot}} \approx \delta_{\text{biomass}}$, then CAP and biomass $\delta^{13}\text{C}$ values would be expected to converge with enhanced recycling. However, such explanation requires that the recycled carbon be incorporated at a biosynthetic stage downstream of simple sugars and prior to the polymerization of CAPs. If the recycled carbon first passed through simple sugars, then no difference in slopes would result among organic compound classes since simple sugars are precursors to proteins and lipids, as well as CAPs.

5. Conclusions: Implications for paleoceanography

412 Our findings indicate that alkenones have greater inherent sensitivity for
413 paleobarometry applications than CAPs due to the steeper slope relating $\delta^{13}\text{C}_{\text{alkenones}}$
414 values to $\mu/[\text{CO}_{2(\text{aq})}]$ (Fig. 1). The relatively constant isotopic depletion in alkenones
415 compared to biomass across four growth conditions supports the conclusions of Popp et
416 al. (1998b) that growth rate does not significantly or systematically influence the isotopic
417 offset between bulk biomass and alkenones. This result upholds the fundamental
418 assumption employed in alkenone-based $p\text{CO}_2$ reconstructions that sedimentary
419 $\delta^{13}\text{C}_{\text{alkenone}}$ measurements can be used to estimate original $\delta^{13}\text{C}_{\text{biomass}}$ values.

420 In contrast, CAPs are not direct analogues or replacements for alkenone
421 biomarkers in the reconstruction of $\delta^{13}\text{C}_{\text{biomass}}$ values, since $\Delta\delta^{13}\text{C}_{\text{biomass-CAP}}$ varies by
422 5.6‰ in our experiments. This is a large variation relative to the limited range of
423 investigated growth and $[\text{CO}_{2(\text{aq})}]$ conditions. However, assuming that our chemostat
424 results are applicable to *in situ* processes in both ancient and modern environments, then
425 alkenones, calcite, and CAPs all recovered from the same sedimentary deposit may
426 together be more useful than alkenones and calcite alone: isotopic measurements of all
427 three cellular constituents would constrain $\mu/[\text{CO}_{2(\text{aq})}]$ with fewer assumptions than
428 current approaches using the $[\text{PO}_4^{3-}]$ -derived “*b*” parameter (Rau et al., 1992, Bidigare et
429 al., 1997). If the alkenones, calcite, and CAPs are related by $\Delta\delta$ values that map onto
430 Fig. 2a and 2b, this information reconstructs $\mu/[\text{CO}_{2(\text{aq})}]$ directly. One advantage of this
431 approach is that it does not require seawater $\delta^{13}\text{C}_{\text{DIC}}$ values, enabling reconstructions
432 from sediments lacking coeval planktonic foraminifera. Another advantage is the
433 potential to recover additional useful information about the coccolithophore community
434 through parallel efforts. CAPs are extracted from fossilized coccoliths, so cell size and

taxonomy information should be recoverable with coccolith calcite and CAP isotope values (Henderiks and Pagani, 2008, Bolton et al., 2012, Bolton and Stoll, 2013, O'Dea et al., 2014, McClelland et al., 2016). The uronic acid contents of CAPs provide complementary information about the internal saturation state of the coccolith vesicle and, by extension, atmospheric CO₂ levels (Lee et al., 2016, Rickaby et al., 2016). Together these strategies point to a way forward for paleobarometry: by analyzing a suite of geologically-preserved constituents, including CAPs, it may be possible to reduce some of the uncertainties inherent to any single-proxy approach. Thus, with additional proxy validation efforts, including cultures and field studies encompassing other species and CO₂ conditions, the carbon isotopic composition of CAPs may provide an important biochemical window into ancient environments.

Acknowledgements

This work was supported by a National Science Foundation Graduate Research Fellowship [grant number DGE1144152, to EBW]; the Gordon and Betty Moore Foundation (to AP); and NASA-NAI CAN6 (to AP; PI Roger Summons, MIT). We thank Susie Carter, Katie Mabbott, and Alan Gagnon for assistance with laboratory analyses and Einat Segev for providing starter cultures and culturing advice.

References

- Abselson, P.H., Hoering, T.C., 1961. Carbon isotope fractionation in formation of amino acids by photosynthetic organisms. *Proceedings of the National Academy of Sciences of the United States of America* 47, 623-632.
- Benthien, A., Zondervan, I., Engel, A., Hefter, J., Terbrüggen, A., Riebesell, U., 2007. Carbon isotopic fractionation during a mesocosm bloom experiment dominated by *Emiliana huxleyi*: Effects of CO₂ concentration and primary production. *Geochimica et Cosmochimica Acta* 71, 1528-1541.
- Bevington P.R., Robinson, D.K., 2003. Data reduction and error analysis for the physical sciences, second ed. McGraw-Hill, New York.
- Bidigare, R.R., Flügge, A., Freeman, K.H., Hanson, K.L., Hayes, J.M., Hollander, D., Jasper, J.P., King, L.L., Laws, E.A., Milder, J., Miller, F.J., Pancost, R., Popp, B.N., Steinberg, P.A., Wakeham, S.G., 1997. Consistent fractionation of ¹³C in nature and in the laboratory: Growth-rate effects in some haptophyte algae. *Global Biogeochemical Cycles* 11, 279-292.
- Bijl, P.K., Houben, A.J.P., Schouten, S., Bohaty, S.M., Sluijs, A., Reichert, G.J., Sinninghe Damsté, D.S., Brinkhuis, H., 2010. Transient middle Eocene atmospheric CO₂ and temperature variations. *Nature* 330, 819-821.
- Bligh, E.G., Dyer, 1959. A rapid method of total lipid extraction and purification. *Canadian Journal of Biochemistry and Physiology* 37, 911-919.
- Boller, A.J., Thomas, P.J., Cavanaugh, C.M., Scott, K.M., 2011. Low stable carbon isotope fractionation by coccolithophore RubisCO. *Geochimica et Cosmochimica Acta* 75, 7200-7207.
- Bolton, C.T., Stoll, H.M., Mendez-Vicente, A., 2012. Vital effects in coccolith calcite: Cenozoic climate pCO₂ drove the diversity of carbon acquisition strategies in coccolithophores? *Paleoceanography* 27, PA4204.
- Bolton, C.T., Stoll, H.M., 2013. Late Miocene threshold response of marine algae to carbon dioxide limitation. *Nature* 500, 558-562.
- Borchard, C., Engel, A., 2012. Organic matter exudation by *Emiliana huxleyi* under simulated future ocean conditions. *Biogeosciences* 9, 3405-3423.
- Borman, A.H., de Jong, E.W., Huizinga, M., Kok, D.J., Westbroek P., Bosch L., 1982. The role in CaCO₃ crystallization of an acid Ca²⁺-binding polysaccharide associated with coccoliths of *Emiliana huxleyi*. *European Journal of Biochemistry* 129, 179-183.
- Bown, P.R., 1987. Taxonomy, biostratigraphy, and evolution of late Triassic-early Jurassic calcareous nannofossils. *Special Papers in Palaeontology* 38, 1-18.
- Brassell, S.C., 2014. Climatic influences on the Paleogene evolution of alkenones. *Paleoceanography* 29, 255-272.
- Chow, J.S., Lee, C., Engel, A., 2015. The influence of acidic polysaccharides, growth rate, and free coccoliths on the coagulation efficiency of *Emiliana huxleyi*. *Marine Chemistry* 175, 5-17.
- Coffin, R.B., Velinsky, D.J., Devereux, R. Price, W.A., Cifuentes, L.A., 1990. Stable carbon isotope analysis of nucleic acids to trace sources of dissolved substrates used by estuarine bacteria. *Applied Environmental Microbiology* 56, 2012-2020.

- De Jong, E.W., Bosch, L., Westbroek, P., 1976. Isolation and characterization of a Ca^{2+} -binding polysaccharide associated with coccoliths of *Emiliania huxleyi* (Lohmann) Kamptner. *European Journal of Biochemistry* 70, 611-612.
- De Vargas, C., Aubry, M.-P., Probert, I., Young, J., 2007. Origin and evolution of coccolithophores: From coastal hunters to oceanic farmers. In: Falkowski, K., Knoll, A. (Eds.), *Evolution of Primary Producers in the Sea*. Elsevier, Boston, pp. 133-163.
- Dickson, A.G., 1990. Standard potential of the reaction: $\text{AgCl(s)} + 1/2\text{H}_2\text{(g)} = \text{Ag(s)} + \text{HCl(aq)}$, and the standard acidity constant of the ion HSO_4^- in synthetic seawater from 273.15 to 318.15 K. *The Journal of Chemical Thermodynamics* 22, 113-127.
- Dickson, A.G., Millero, F.J., 1987. A comparison of the equilibrium constants for the dissociation of carbonic acid in seawater media. *Deep Sea Research Part I* 34, 1733-1743.
- Dickson, A.G., Sabine, C.L., Christian, J.R., 2007. Guide to best practices for ocean CO_2 measurements. *PICES Special Publication* 3, 1-191.
- Farrimond P., Eglinton, G., Brassell, S.C., 1986. Alkenones in Cretaceous black shales, Blake-Bahama Basin, western North Atlantic. *Organic Geochemistry* 10, 897-903.
- Fichtinger-Schepman, A.M., Kamerling, J.P., Versluis, C., Vliegenthart, F.G., 1981. Structural studies of the methylated, acidic polysaccharide associated with coccoliths of *Emiliania huxleyi* (Lohmann) Kamptner, 1981. *Carbohydrate Research* 93, 105-123.
- Freeman, K.H., Hayes, J.M., 1992. Fractionation of carbon isotopes by phytoplankton and estimates of ancient CO_2 levels. *Global Biogeochemical Cycles* 6, 185-198.
- Goericke, R., Montoya, J., Fry, B., 1994. Physiology of isotopic fractionation in algae and cyanobacteria. In: Lajtha, K., Michener, R. (Eds.), *Stable Isotopes in Ecology and Environmental Science*. Blackwell Scientific Publications, Oxford, pp. 187-221.
- Gran, G., 1952. Determination of the equivalence point in potentiometric titrations, Part II. *Analyst* 77, 661-671.
- Guillard, R.R.L., Hargraves, P.E., 1993. *Stichochrysis immobilis* is a diatom, not a chrysophyte. *Phycologia* 32, 234-236.
- Halsey, K.H., Milligan, A.J., Behrenfeld, M.J., 2011. Linking time-dependent carbon-fixation efficiencies in *Dunaliella tertiolecta* (chlorophyceae) to underlying metabolic pathways. *Journal of Phycology* 47 66-76.
- Hayes, J.M., 2001. Fractionation of carbon and hydrogen isotopes in biosynthetic processes. *Reviews in Mineralogy and Geochemistry* 43, 225-277.
- Henderiks, J., 2008. Coccolithophore size rules – Reconstructing ancient cell geometry and cellular calcite quota from fossil coccoliths. *Marine Micropaleontology* 67, 143-154.
- Henriksen, K., Stipp, S.L.S., 2009. Controlling biomineralization: The effect of solution composition on coccolith polysaccharide functionality. *Crystal Growth and Design* 9, 2088-2097.
- Hermoso, M., Rickaby, R.E.M., Minoletti, F., Diester-Haas, L., 2009. The Middle Miocene paleoceanographic events as seen by the chemistry of calcareous nannofossils in SW Pacific Ocean. *Eos Transactions AGU* 90, PP41A-1498.

544 Hermoso, M., 2014. Coccolith-derived isotopic proxies in palaeoceanography: where
 545 geologists need biologists. *Cryptogamie, Algologie* 35, 323-351.
 546 Hermoso, M., Minoletti, F., Aloisi, G., Bonifacie, M., McClelland, H.L.O., Labourdette,
 547 N., REnforth, P., Chaduteau, C., Rickaby, R.E.M., 2016a. An explanation for the
 548 ^{18}O excess in Noelaerhabdaceae coccolith calcite. *Geochimica et Cosmochimica*
 549 *Acta* 189, 132-142.
 550 Hermoso, M., Chan, I.Z.X., McClelland, H.L.O., Heureux, A.M.C., Rickaby, R.E.M.,
 551 2016b. Vanishing coccolith vital effects with alleviated carbon limitation.
 552 *Biogeoscience* 13, 301-312.
 553 Holtz, L.-M., Wolf-Gladrow, D., Thoms, S., 2017. Stable carbon isotope signals in
 554 particulate organic and inorganic carbon of coccolithophores – A numerical
 555 model study for *Emiliani huxleyi*. *Journal of Theoretical Biology* 420, 117-127.
 556 Jasper, J.P., Hayes, J.M., 1990. A carbon isotope record of CO_2 levels during the late
 557 Quaternary. *Nature* 347, 462-464.
 558 Jasper, J.P., Hayes, J.M., Mix, A.C., Prahl, F.G., 1994. Photosynthetic fractionation of ^{13}C
 559 and concentrations of CO_2 in the central equatorial Pacific during the last 225,000
 560 years. *Paleoceanography* 9, 781-898.
 561 Katz, A., Bonifacie, M., Hermoso, M., Cartigny, P., Calmels, D., 2017.
 562 Laboratory-grown coccoliths exhibit no vital effect in clumped isotope (Δ_{47})
 563 composition on a range of geologically relevant temperatures. *Geochimica et*
 564 *Cosmochimica Acta* 208, 335-353.
 565 Keller, K., Morel, F.M.M., 1999. A model of carbon isotopic fractionation and active
 566 carbon uptake in phytoplankton. *Marine Ecological Progress Series* 182, 295-298.
 567 Kok, D.J., Blomen, L.J.M.J., Westbroek, P., Bijvoet, O.L.M., 1986. Polysaccharide from
 568 coccoliths (CaCO_3 biomineral): influence on crystallization of calcium oxalate
 569 monohydrate. *European Journal of Biochemistry* 158, 167-172.
 570 Kottmeier, D.M., Rokitta, S.D., Tortell, P.D., Rost, B., 2014. Strong shift from HCO_3^- to
 571 CO_2 uptake in *Emiliana huxleyi* with acidification: new approach unravels
 572 acclimation versus short-term pH effects. *Photosynthesis Research* 121, 265-275.
 573 Laws, E.A., Bidigare, R.R., Popp, B.N., 1997. Effect of growth rate and CO_2
 574 concentration on carbon isotope fractionation by the marine diatom
 575 *Phaeodactylum tricornutum*. *Limnology and Oceanography* 42, 1552-1560.
 576 Laws, E.A., Popp, B.N., Bidigare, R.R., Riebesell, U., Burkhardt, S., Wakeham, S.G.,
 577 2001. Controls on the molecular distribution and carbon isotopic composition of
 578 alkenones in certain haptophyte algae. *Geochemistry Geophysics Geosystems* 2,
 579 2000GC000057.
 580 Lee, R.B.Y., Mavridou, D.A.I., Papadakos, G., McClelland, H.L.O., Rickaby, R.E.M.,
 581 2016. The uronic acid content of coccolith-associated polysaccharides provides
 582 insight into coccolithogenesis and past climate. *Nature Communications* 7, DOI:
 583 10.1038/ncomms13144.
 584 Lewis, E., Wallace, D., 1998. Program developed for CO_2 system calculations: Oak
 585 Ridge TN Oak Ridge National Laboratory Environmental Sciences Division, v.
 586 4735.
 587 Macko, S.A., Helleur, R., Hartley, G., Jackman, P., 1990. Diagenesis of organic matter –
 588 a study using stable isotopes of individual carbohydrates. *Organic Geochemistry*
 589 16, 1129-1137.

- Marchal, O., Cacho, I., Stocker, T.F., Grimalt, J.O., Calvo, E., Martrat, B., Shackleton, N., Vautravers, M., Cortijo, E., van Kreveland, S., Andersson, C., Koc, N., Chapman, M., Saffi, L., Duplessy, J.C., Sarnthein, M., Turon, J.L., Duprat, J., and Jansen, E., 2002. Apparent long-term cooling of the sea surface in the northeast Atlantic and Mediterranean during the Holocene. *Quaternary Science Reviews* 21, 455-483.
- Marsh, M.E., 1994. Polyanion-mediated mineralization—assembly and reorganization of acidic polysaccharides in the Golgi system of a coccolithophorid alga during mineral deposition. *Protoplasma* 177, 108-122.
- Marsh, M.E., 2003. Regulation of CaCO₃ formation in coccolithophores. *Comparative Biochemistry and Physiology Part B: Biochemistry and Molecular Biology* 136, 743-754.
- Marsh, M.E., Ridall, A.L., Azadi, P., Duke, P.J., 2002. Galacturonomannan and golgi-derived membrane linked to growth and shaping of biogenic calcite. *Journal of Structural Biology* 139, 39-45.
- McClelland, H.L.O., Hermoso, M., Bruggeman, J., Rickaby, R.E.M., 2015. Towards a unifying theory for carbon isotopic partitioning in coccolithophores: Implications for paleo-proxies. *Goldschmidt Abstracts*, 2069.
- McClelland, H.L.O., Barbarin, N., Beaufort, L., Hermoso, M., Ferretti, P., Greaves, M., Rickaby, R.E.M., 2016. Calcification response of a key phytoplankton family to millennial-scale environmental change. *Scientific Reports* 6, 34263.
- McClelland, H.L.O., Bruggeman, J., Hermoso, M., Rickaby, R.E.M., 2017. The origin of carbon isotope vital effects in coccolith calcite. *Nature Communications* 8, DOI: 10.1038/ncomms14511.
- Mehrbach, C., Culbertson, C.H., Hawley, J.E., Pytkowicz, R.M., 1973. Measurement of the apparent dissociation constants of carbonic acid in seawater at atmospheric pressure. *Limnology and Oceanography* 18, 897-907.
- Monson, K.D., Hayes, J.M., 1982. Carbon isotopic fractionation in the biosynthesis of bacterial fatty acids—Ozonolysis of unsaturated fatty acids as a means of determining the intramolecular distribution of carbon isotopes. *Geochimica et Cosmochimica Acta* 46, 139-149.
- Mook, W.G., Bommerson, J.C., Staverman, W.H., 1974. Carbon isotope fractionation between dissolved bicarbonate and gaseous carbon dioxide. *Earth and Planetary Science Letters* 22, 169-176.
- O'Dea, S.A., Gibbs, S.J., Bown, P.R., Young, J.R., Poulton, A.J., Newsam, C., Wilson, P.A., 2014. Coccolithophore calcification response to past ocean acidification and climate change. *Nature Communications* 5, DOI:10.1038/ncomms6363.
- Pagani, M., Zachos, J., Freeman, K.H., Bohaty, S., Tipler, B., 2005. Marked decline in atmospheric carbon dioxide concentrations during the Paleogene. *Science* 309, 600-603.
- Perrin, L., Probert, I., Langer, G., Aloisi, G., 2016. Growth of the coccolithophore *Emiliana huxleyi* in light- and nutrient-limited batch reactors: relevance for the BIOSOPE deep ecological niche of coccolithophores. *Biogeosciences* 13, 5983-6001.

- Popp, B.N., Laws, E.A., Bidigare, R.R., Dore, J.E., Hanson, K.L., Wakeham, S.G., 1998a. Effect of phytoplankton cell geometry on carbon isotopic fractionation. *Geochimica et Cosmochimica Acta* 62, 69–77.
- Popp, B.N., Kenig, F., Wakeham, S.G., Laws, E.A., Bidigare, R.R., 1998b. Does growth rate affect ketone unsaturation and intracellular carbon isotopic variability in *Emiliana huxleyi*? *Paleoceanography* 13, 35–41.
- Rickaby, R.E.M., Bard, E., Sonzogni, C., Rostek, F., Beaufort, L., Barker, S., Rees, G., Schrag, D.P., 2007. Coccolith chemistry reveals secular variations in the global ocean carbon cycle? *Earth and Planetary Science Letters* 253, 83–95.
- Rickaby, R.E.M., Hermoso, M., Lee, R.B.Y., Rae, B.D., Heures, A.M.C., Balestreri, C., Chakravarti, L., Schroeder, D.C., Brownlee, C., 2016. Environmental carbonate chemistry selects for phenotype of recently isolated strains of *Emiliana huxleyi*. *Deep-Sea Research II* 127, 28–40.
- Riebesell, U., Revill, A.T., Holdsworth, D.G., Volkman, J.K., 2000. The effects of varying CO₂ concentration on lipid composition and carbon isotope fractionation in *Emiliana huxleyi*. *Geochimica et Cosmochimica Acta* 64, 4179–4192.
- Romanek, C.S., Grossman, E.L., Morse, J.W., 1992. Carbon isotopic fractionation in synthetic aragonite and calcite: Effects of temperature and precipitation rate. *Geochimica et Cosmochimica Acta* 56, 419–430.
- Rost, B., Zondervan, I., Riebesell, U., 2002. Light-dependent carbon isotope fractionation in the coccolithophorid *Emiliana huxleyi*. *Limnology and Oceanography* 47, 120–128.
- Sakata, S., Hayes, J.M., McTaggart, A.R., Evans, R.A., Leckrone, K.J., Togasaki, R.K., 1997. Carbon isotopic fractionation associated with lipid biosynthesis by a cyanobacterium: Relevance for interpretation of biomarker records. *Geochimica et Cosmochimica Acta* 61, 5379–5389.
- Schouten, S., Klein Breteler, W.C.M., Blokker, P., Schogt, N., Rupstra, I.C., Grice, K., Baas, M., Sinninghe Damsté, J.S., 1998. Biosynthetic effects on the stable carbon isotopic compositions of algal lipids: Implications for deciphering the carbon isotopic biomarker record. *Geochimica et Cosmochimica Acta* 62, 1397–1406.
- Schulz, K.G., Rost, B., Burkhardt, S., Riebesell, U., Thoms, S., Wolf-Gladrow, D.A., 2007. The effect of iron availability on the regulation of inorganic carbon acquisition in the coccolithophore *Emiliana huxleyi* and the significance of cellular compartmentation for stable carbon isotope fractionation. *Geochimica et Cosmochimica Acta* 71, 5301–5312.
- Seki, O., Foster, G.L., Schmidt, D.N., Mackensen, A., Kawamura, K., Pancost, R.D., 2010. *Earth and Planetary Science Letters* 292, 201–211.
- Stoll, H.M., 2005. Limited range of interspecific vital effects in coccolith stable isotopic records during the Paleocene-Eocene thermal maximum. *Paleoceanography* 20, DOI: 10.1029/2004PA001046.
- Strickland, J.D.H., Parsons, T.R., 1968. Determination of reactive phosphorus. In: A practical handbook of seawater analysis. Fisheries Research Board of Canada, Bulletin 167, pp. 49–56.
- Taylor, A.R., Brownlee, C., Wheeler G., 2017. Coccolithophore cell biology: chalking up progress, *Annual Review of Marine Science* 9, 283–310.

- Tchernov, D., Gruber, D.F., Irwin, A., 2014. Isotopic fractionation of carbon in the coccolithophorid *Emiliana huxleyi*. Marine Ecology Progress Series 508, 53-66.
- Teece, M.A., Fogel, M.L., 2007. Stable carbon isotope biogeochemistry of monosaccharides in aquatic organisms and terrestrial plants. Organic Geochemistry 38, 458-473.
- Thierstein, H.R., Geitzenauer, K.R., Molfino, B., Shackleton, N.J., 1977. Global synchronicity of late Quaternary coccolith datum levels validation by oxygen isotopes. Geology 5, 400-404.
- Van Dongen, B.E., Schouten, S., Sinninghe Damsté, 2002. Carbon isotope variability in monosaccharides and lipids of aquatic algae and terrestrial plants 232, 83-92.
- Van Heuven, S., Pierrot, D., Rae, J.W.B., Lewis, E., Wallace, D.W.R., 2011. MATLAB program developed for CO₂ system calculations. Carbon Dioxide Information Analysis Center, Oak Ridge National Laboratory.
- Volkman, J.K., Eglinton, G., Corner, E.D.S., Sargent, J.R., 1980. Novel unsaturated straight-chain C₃₇-C₃₉ methyl and ethyl ketones in marine sediments and a coccolithophore *Emiliana huxleyi*. Physics and Chemistry of the Earth, 12, 219-227.
- Westbroek, P., Brown C.W., van Bleijswijk, J., Brownlee, C., Brummer, G.J., Conte, M., Egge, J., Fernández, E., Jordan, R., Knappertsbusch, M., Stefels, J., Veldhuis, M., van der Wal, P., Young, J., 1993. A model system approach to biological climate forcing—the example of *Emiliana huxleyi*. Global Planetary Change 8, 27-46.
- Wilkes, E.B., Carter, S.J., Pearson, A., 2017. CO₂-dependent carbon isotope fractionation in the dinoflagellate *Alexandrium tamarense*. Geochimica et Cosmochimica Acta 212, 48-61.
- Wong, W., Sackett, W.M., Benedict, C.R., 1975. Isotope fractionation in photosynthetic bacteria during carbon dioxide assimilation. Plant Physiology 55, 475-479.
- Young, J.R., Henricksen, K., 2003. Biomineralization vesicles: the calcite of coccoliths. Reviews in Mineralogy and Geochemistry 54, 189-214.
- Zeebe, R.E., Wolf-Gladrow, D., 2001. CO₂ in seawater: Equilibrium, kinetics, isotopes. Elsevier, Amsterdam.
- Zhang, J., Quay, P.D., Wilbur, D.O., 1995. Carbon isotope fractionation during gas-water exchange and dissolution of CO₂ 59, 107-114.
- Zhang, J.-Z., Fischer, C.J., 2006. A simplified resorcinol method for direct spectrophotometric determination of nitrate in seawater. Marine Chemistry 99, 220-226.
- Zhang, Y.G., Pagani, M., Liu, Z., Bohaty, S.M., Deconto, R., 2013. A 40-million-year history of atmospheric CO₂. Philosophical Transactions of the Royal Society A 371, 20130096.
- Ziveri, P., Stoll, H., Probert, I., Klaas, C., Geisen, M., Ganssen, G.M., Young, J., 2003. Stable isotope ‘vital effects’ in coccolith calcite. Earth and Planetary Science Letters 210, 137-149.

Tables & Figures

Table 1. Experimental conditions and isotopic data for *E. huxleyi*^{a,b}

Expt #	[CO _{2(aq)}] ($\mu\text{mol kg}^{-1}$)	μ^c (d^{-1})	$\delta^{13}\text{C}_{\text{calcite}}$ (‰)	$\delta^{13}\text{C}_{\text{biomass}}$ (‰)	$\delta^{13}\text{C}_{\text{CAP}}$ (‰)	$\delta^{13}\text{C}_{\text{alkenone}}$ (‰)
1	17.6 \pm 1.2	0.20 \pm 0.01	-15.44 \pm 0.01	-48.2 \pm 1.4	-38.2 \pm 0.2	-51.5 \pm 1.0
2	14.0 \pm 0.4	0.40 \pm 0.01	-12.90 \pm 0.01	-45.7 \pm 0.1	-37.3 \pm 0.5	-49.8 \pm 0.9
3	11.9 \pm 0.5	0.48 \pm 0.01	-10.44 \pm 0.01	-42.9 \pm 0.3	-35.4 \pm 0.5	-46.4 \pm 0.5
4	10.7 \pm 0.6	0.62 \pm 0.01	-8.26 \pm 0.01	-39.5 \pm 0.9	-34.9 \pm 0.5	-42.4 \pm 0.5

^aValues reflect the mean of steady-state conditions, $\pm 1\sigma$.

^bThe order in which the experiments were performed is: 2, 3, 1, 4.

^cValues and associated errors correspond to the dilution rates applied to the chemostat system, equaling μ at steady-state.

Table 2. Isotopic offsets between cellular pools (‰).^a

Expt #	$\Delta\delta^{13}\text{C}_{\text{calcite-CAP}}$	$\Delta\delta^{13}\text{C}_{\text{CAP-biomass}}$	$\Delta\delta^{13}\text{C}_{\text{biomass-alkenone}}$	$\Delta\delta^{13}\text{C}_{\text{calcite-biomass}}$	$\Delta\delta^{13}\text{C}_{\text{alkenone-CAP}}$
1	22.7 ± 0.2	10.1 ± 1.4	3.3 ± 1.7	32.8 ± 1.4	-13.4 ± 1.0
2	24.4 ± 0.5	8.4 ± 0.5	4.2 ± 0.9	32.8 ± 0.1	-12.6 ± 1.1
3	24.9 ± 0.5	7.5 ± 0.6	3.5 ± 0.6	32.5 ± 0.3	-11.0 ± 0.7
4	26.7 ± 0.5	4.5 ± 1.0	2.9 ± 1.0	31.2 ± 0.9	-7.4 ± 0.7
Mean	24.7	8	3.5	32.3	-11.1
SD	1.6	2	0.5	0.7	2.6

^aValues are $\pm 1\sigma$ propagated error.

Table 3. Four carbon allocation scenarios consistent with δ_{biomass} and δ_{CAP} measurements.

Relative δ		Expt #	δ_{biomass}	f_{lip}	δ_{lip}	f_{prot}	δ_{prot}	f_{carb}	δ_{carb}	f_{CAP}	δ_{CAP}	f_{sacc}	δ_{sacc}	% carbon allocation to CAPs
Prot^a	0	1	-48.2	0.25	-52.2	0.50	-48.2	0.25	-44.2	0.14	-38.2	0.86	-45.2	3.5
Carb^a	4	2	-45.7	0.25	-49.7	0.50	-45.7	0.25	-41.7	0.37	-37.3	0.63	-44.3	9.3
Lip^a	-4	3	-42.9	0.25	-46.9	0.50	-42.9	0.25	-38.9	0.50	-35.4	0.50	-42.4	12.5
$\Delta\delta_{\text{CAP-sacc}}$^a	7	4	-39.5	0.25	-43.5	0.50	-39.5	0.25	-35.5	0.91	-34.9	0.09	-41.9	22.8
Prot	1	1	-48.2	0.25	-52.2	0.63	-47.2	0.13	-45.2	0.13	-38.2	0.87	-46.2	1.6
Carb	3	2	-45.7	0.25	-49.7	0.63	-44.7	0.13	-42.7	0.33	-37.3	0.67	-45.3	4.1
Lip	-4	3	-42.9	0.25	-46.9	0.63	-41.9	0.13	-39.9	0.44	-35.4	0.56	-43.4	5.5
$\Delta\delta_{\text{CAP-sacc}}$	8	4	-39.5	0.25	-43.5	0.63	-38.5	0.13	-36.5	0.80	-34.9	0.20	-42.9	10.0
Prot	0	1	-48.2	0.25	-52.2	0.42	-47.2	0.33	-45.2	0.13	-38.2	0.87	-46.2	4.3
Carb	3	2	-45.7	0.25	-49.7	0.42	-44.7	0.33	-42.7	0.33	-37.3	0.67	-45.3	10.9
Lip	-4	3	-42.9	0.25	-46.9	0.42	-41.9	0.33	-39.9	0.44	-35.4	0.56	-43.4	14.5
$\Delta\delta_{\text{CAP-sacc}}$	8	4	-39.5	0.25	-43.5	0.42	-38.5	0.33	-36.5	0.80	-34.9	0.20	-42.9	26.4
Prot	1	1	-48.2	0.25	-52.2	0.50	-47.2	0.25	-46.2	0.11	-38.2	0.89	-47.2	2.8
Carb	2	2	-45.7	0.25	-49.7	0.50	-44.7	0.25	-43.7	0.29	-37.3	0.71	-46.3	7.3
Lip	-4	3	-42.9	0.25	-46.9	0.50	-41.9	0.25	-40.9	0.39	-35.4	0.61	-44.4	9.8
$\Delta\delta_{\text{CAP-sacc}}$	9	4	-39.5	0.25	-43.5	0.50	-38.5	0.25	-37.5	0.71	-34.9	0.29	-43.9	17.8

^aScenario described in the body of the text.

Figure Captions

Figure 1. The $\delta^{13}\text{C}$ values (‰) of coccolith calcite (black triangles), CAPs (grey circles), bulk biomass (white squares), and alkenones (black diamonds) (a) as a function of the ratio of growth rate (μ) to CO_2 concentration ($[\text{CO}_{2(\text{aq})}]$), (b) comparing $\delta^{13}\text{C}_{\text{alkenone}}$ values to $\delta^{13}\text{C}_{\text{biomass}}$ and $\delta^{13}\text{C}_{\text{calcite}}$ values, with slopes of approximately 1, and (c) comparing $\delta^{13}\text{C}_{\text{CAP}}$ values to $\delta^{13}\text{C}_{\text{biomass}}$ and $\delta^{13}\text{C}_{\text{calcite}}$, showing slopes of approximately 0.5.

Figure 2. Isotopic fractionations ($\Delta\delta$ values, ‰) between compound classes, calculated as simple linear differences and plotted versus $\mu/[\text{CO}_{2(\text{aq})}]$: (a) $\Delta\delta^{13}\text{C}_{\text{calcite-CAP}}$, (b) $\Delta\delta^{13}\text{C}_{\text{CAP-biomass}}$, (c) $\Delta\delta^{13}\text{C}_{\text{biomass-alkenone}}$, (d) $\Delta\delta^{13}\text{C}_{\text{calcite-biomass}}$. Error bars represent $\pm 1\sigma$ propagated error. Note: all vertical axes span 12‰ ranges, but with different values.

Figure 3. Predicted cellular carbon allocation to major organic compound classes in *E. huxleyi*. Arrow widths correspond to calculated fractional fluxes (f). Relative shading intensities indicate the measured or predicted isotopic offsets between the organic carbon pools, including the bulk biomass. (a) Cells from Experiment #1 (left; lowest $\mu/[\text{CO}_{2(\text{aq})}]$) preferentially allocate carbon within the carbohydrate pool to saccharides other than CAPs. Cells from Experiment #4 (right; highest $\mu/[\text{CO}_{2(\text{aq})}]$) allocate more carbon to CAP synthesis. (b) Percentages of fixed carbon allocated to CAPs for each experiment, calculated for four plausible combinations of δ_{prot} and δ_{carb} model inputs. Regardless of choice, carbon allocation to CAPs is expected to increase from Experiment #1 to Experiment #4 (with increasing $\mu/[\text{CO}_{2(\text{aq})}]$). Abbreviations: *PDH* = pyruvate dehydrogenase, *OAA* = oxaloacetate.

Figure 1.

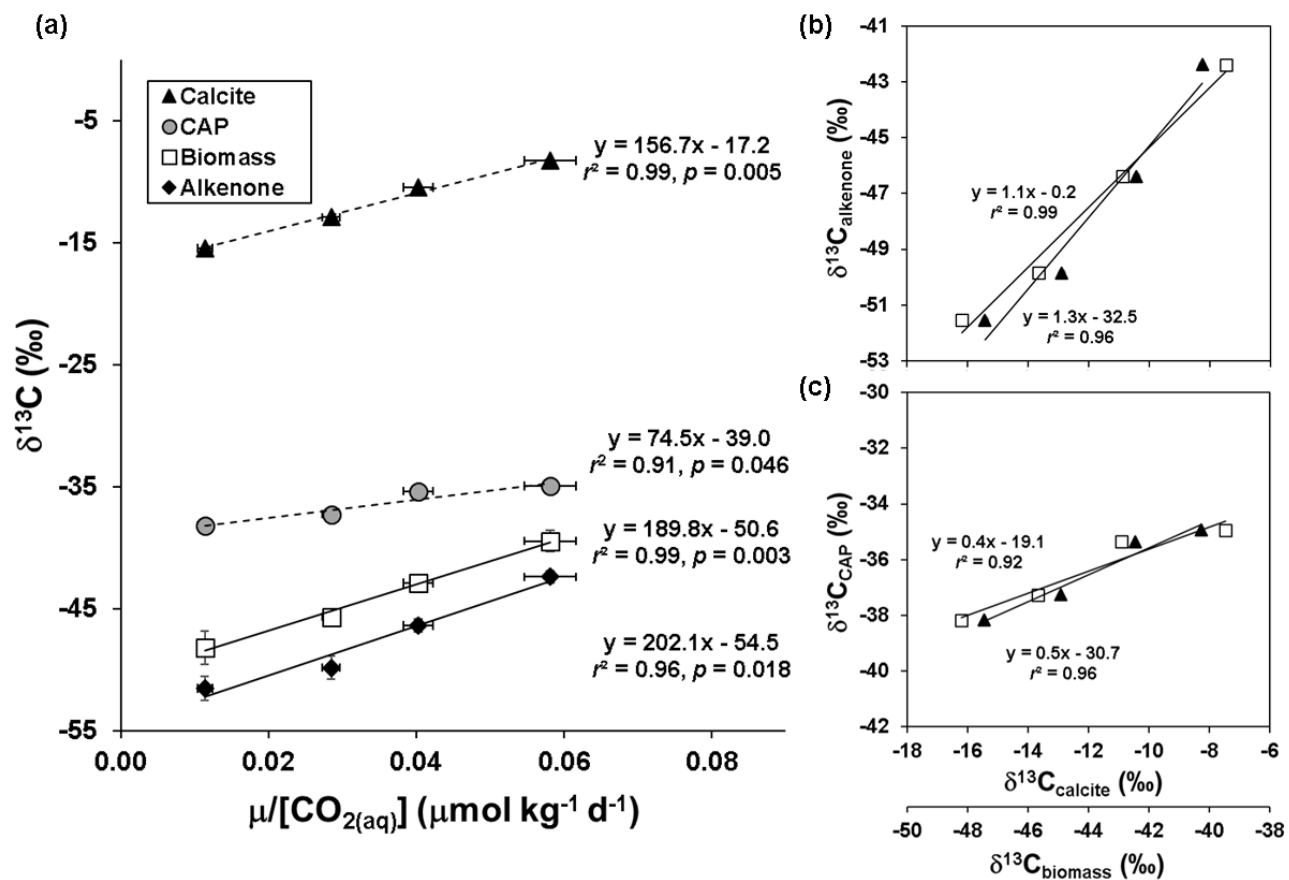


Figure 2.

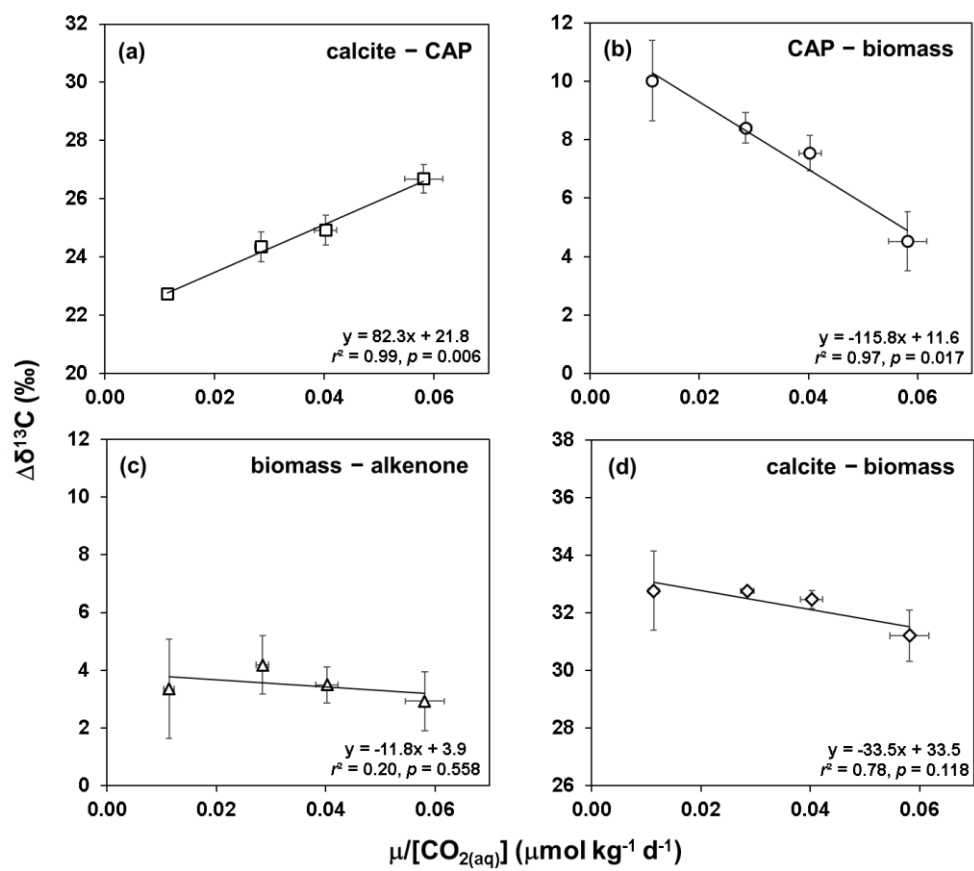
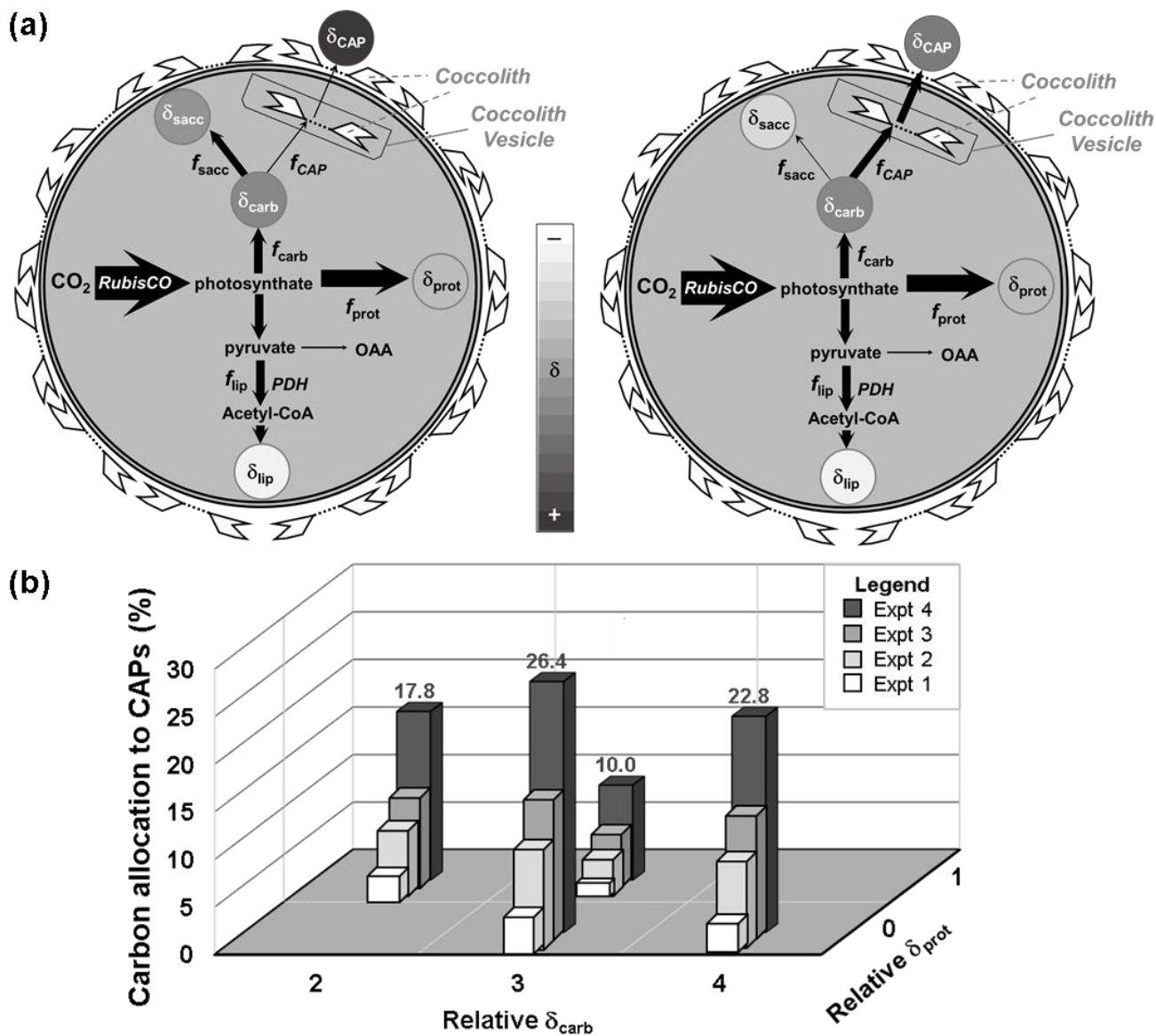


Figure 3.



Supplementary Material

[Click here to download Supplementary Material: Supplemental online information for CAPsmanuscript.docx](#)